RMP Colloquia

This section, begun in January 1992, contains short articles intended to describe recent research of interest to a broad audience of physicists. It will concentrate on research at the frontiers of physics, especially on concepts able to link many different subfields of physics. Responsibility for its contents and readability rests with the Advisory Committee on Colloquia, U. Fano, chair, Robert Cahn, S. Freedman, P. Parker, C. J. Pethick, and D. L. Stein. Prospective authors are encouraged to communicate with Professor Fano or one of the members of this committee.

Observing electron motion in solids

M. Vos and I. E. McCarthy

Electronic Structure of Materials Centre, Flinders University of South Australia, GPO Box 2100, Adelaide, S.A. 5001, Australia

We describe an experimental technique that allows for the direct determination of the motion (i.e., the momentum) of electrons in atoms, molecules, and solids. This $(e,2e)$ technique centers on a fast electron's ejecting a second electron from a target. Precise spectroscopy of both electrons' final energies and momenta provides very significant information on the second electron's initial state. Decades of past $(e,2e)$ studies on single-molecule states have now progressed into studies of condensed matter. The interpretation of these experiments is mediated in this colloquium by analysis of intermediate models in the form of chainlike molecules.

CONTENTS

I. INTRODUCTION

The $(e,2e)$ technique has served extensively to study wave functions of atoms and molecules. In these gas-phase experiments a fast electron ($\simeq 1$ keV or higher) scatters from an atomic or molecular electron, ejecting that electron. The scattered and ejected electrons are then detected *in coincidence*, and analyzed for their energy and momenta. These kinematically complete experiments serve to determine the binding energy ε and the momentum $\mathbf{q}$ of the ejected electron *before* the scattering event, thus providing the spectral momentum density $|\phi(\varepsilon,\mathbf{q})|^2$. Therefore $(e,2e)$ spectroscopy is often called electron-momentum spectroscopy. For reviews of this technique as applied to molecules see McCarthy and Weigold (1991) or Coplan *et al.* (1994).

A crystal is invariant under translations by a lattice vector. As a consequence the solution of the Hamiltonian can be written as a Bloch function, i.e.,

$$\psi_{\mathbf{k}}(\mathbf{r})=e^{i\mathbf{k}\cdot\mathbf{r}}u_{\mathbf{k}}(\mathbf{r})=\sum_{\mathbf{G}}c_{\mathbf{G}}e^{i(\mathbf{k}+\mathbf{G})\cdot\mathbf{r}}\ . \tag{1}$$

Here $u_{\mathbf{k}}(\mathbf{r})$ is a function with the periodicity of the lattice and can be expressed in a Fourier series with summation over all reciprocal-lattice vectors $\mathbf{G}$. The vector $\mathbf{k}$ is called the crystal momentum. Thus an eigenfunction of the Hamiltonian is a sum of components with wave number $\mathbf{k}+\mathbf{G}$, and in principle each of these components can be used as a label of the wave function. There are different conventions in use for plotting the relation between energy and crystal momentum. If the energy-momentum relation is plotted for $\mathbf{k}+\mathbf{G}$ in the first Brillouin zone only, the band structure is represented in the *reduced* zone scheme. Alternatively one can plot the energy-momentum relation for all $\mathbf{k}+\mathbf{G}$ values, by repeating the structure of the first zone. This is called the *repeated* zone scheme. Finally there is almost always one component $\mathbf{k}+\mathbf{G}$ in Eq. (1) that dominates the others. If one plots the energy-momentum relation for the dominant $\mathbf{k}+\mathbf{G}$ component only, one uses the *extended* zone scheme.

Under favorable circumstances the relation between energy and crystal momentum can be measured for a single crystal by angle-resolved ultraviolet photoelectron spectroscopy. Here we explain the application of $(e,2e)$ to solids and point out the major differences between the measurement of momentum by $(e,2e)$ and of crystal momentum by photoemission.

The relation between observations of $(e,2e)$ spectroscopy and the theory of the solid state has been understood for quite some time (see, for example, Neudachin *et al.*, 1968; Levin *et al.*, 1972; Gao *et al.*, 1988). In these scattering experiments, based on energy and momentum conservation, one measures the real momentum of the electron. This insight has been a major impetus for different research groups to develop $(e,2e)$ experiments on solids during the past 20 years. The first pioneering experiments were carried out by Amaldi *et al.* in 1969, followed by Camilloni *et al.* in 1972, who were the first to observe a momentum density, in this case for the core state of solid carbon. These experiments were hampered by poor energy resolution (± 100 eV). Energy resolution

 0034-6861/95/67(3)/713(11)/$08.65 ©1995 The American Physical Society

improved to 16 eV in the experiments reported by Persiantseva *et al.* (1979). Further improvements by Ritter and co-workers (1984) made it possible to resolve dispersion in the valence band of carbon with an energy resolution of 8 eV. The count rate was improved by Hayes *et al.* using multichannel energy detection with a resolution of 4.5 eV. The present spectrometer using multiple energy *and* multiple angle detection, as described by Storer *et al.* (1994), again has a much improved count rate and energy resolution (2 eV).

These spectrometer developments have led to a series of new experiments with improved resolution and statistics. The technique proved capable of addressing a range of questions in solid-state physics. Vos *et al.* (1994) and Cai *et al.* (1995a) measured crystal band structures. Caprari *et al.* (1994) studied the 1*s* core-level momentum distribution of a carbon film. Application of this technique to disordered materials is of special interest. Measurements of various stages of recrystallization of amorphous carbon films were made by Vos, Storer, *et al.* (1995b). Amorphous silicon was studied by Vos, Storer, *et al.* (1995a) and SiC by Cai *et al.* (1995b). Finally oxygen adsorbed on amorphous carbon was studied by Vos, Canney, *et al.* (1995b). Thus we think it desirable for workers in these and related fields to appreciate the potential of $(e,2e)$ studies on solids. This paper should also provide a wider audience with an intuitive understanding of the $(e,2e)$ technique as applied to solids. To aid the understanding of electronic structure we derive many of the familiar results of band-structure theory in terms of molecular orbitals in momentum representation, building an elegant bridge between molecular and solid-state physics.

II. THE $(e,2e)$ TECHNIQUE AS APPLIED TO ATOMS AND MOLECULES

In $(e,2e)$ measurements an incoming electron ionizes the target, and the scattered and ejected electrons are detected in coincidence. Achieving sufficient momentum and energy resolution requires a well-collimated monoenergetic electron beam (energy E_0, momentum $\mathbf{p}_0$) impinging on a target. Some electrons will scatter from a target electron. For small momentum transfers, dipole selection rules apply. Most electron energy-loss spectroscopy (EELS) data are collected in this regime, a field thoroughly reviewed by Egerton (1986) and not discussed here. Instead, $(e,2e)$ spectroscopy, as described here, involves large momentum transfers, which allow us to describe the collision between impinging and target electrons as a *binary* collision. The energy and momentum transferred by the impinging electron eject the target electron.

We choose atomic units (a.u.) setting $\hbar=1$, and thereby equating momenta and wave numbers. (1 a.u. as a unit of length corresponds to 0.529 Å, 1 a.u. of momentum corresponds to 1.89 Å^{-1}). The label $\mathbf{p}$ will refer to electron momenta as determined outside a molecule or crystal and $\mathbf{q}$ to the real momentum of the electron to be ejected in the molecule or crystal immediately before the scattering event, whereas $\mathbf{k}$ refers to the crystal momentum. Scattered and ejected electrons are detected *in coincidence,* determining their energies and momenta (E_s and $\mathbf{p}_s$ for the slower of the two electrons, E_f and $\mathbf{p}_f$ for the faster one).

Comparing the momenta and energies of the scattered and ejected electrons with the momentum and energy of the incident electron yields the magnitudes of the momentum and binding energy of the ejected electron *before* the collision. We thus determine the binding energy ε as

$$\varepsilon=E_0-E_s-E_f \ . \tag{2}$$

At sufficiently high energies the free electrons can be treated as plane waves, and the momentum of the target electron before the collision is given by

$$\mathbf{q}=\mathbf{p}_s+\mathbf{p}_f-\mathbf{p}_0 \ . \tag{3}$$

A complete description of the kinematics of each ionizing event is thus obtained, from which the spectral momentum density $|\phi(\varepsilon,\mathbf{q})|^2$ can be derived.

The cross section at energy ε for the $(e,2e)$ process of scattering from electrons in an orbital a with binding energy ε_a is given in the plane-wave Born approximation by

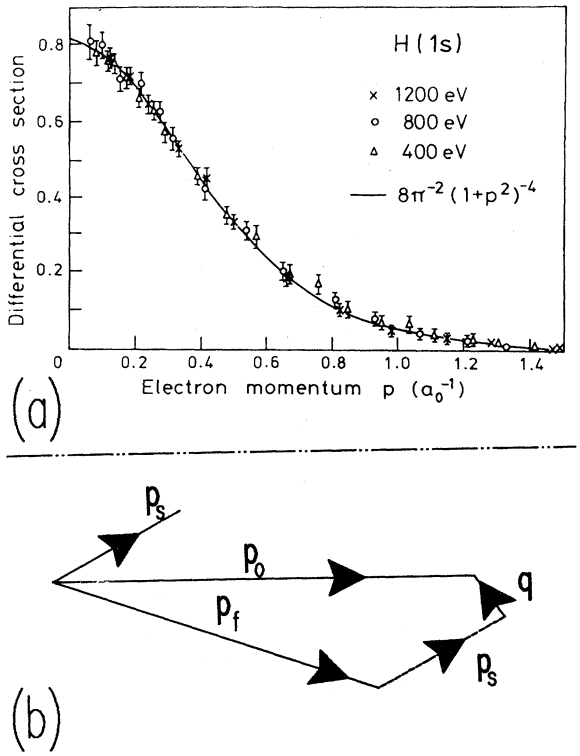

FIG. 1. The $(e,2e)$ results for atomic hydrogen: (a) The arbitrarily normalized, experimentally determined momentum density $|\phi(\mathbf{q})|^2$ for atomic hydrogen. Results for the different energies E_0 are indicated. Also shown is the *exact* theoretical solution of the momentum density of the hydrogen atom (solid line), from Lohmann and Weigold (1981); (b) The different momentum components involved in an $(e,2e)$ experiment.

$$\frac{d^5\sigma}{d\Omega_f d\Omega_s dE_f} = (2\pi)^4 \frac{p_f p_s}{p_0} f_{ee} |\phi_a(\mathbf{q})|^2 \delta(\varepsilon - \varepsilon_a) , \quad (4)$$

where ε_a stands for the binding energy of orbital a and f_{ee} for the Mott cross section (which includes the exchange contribution),

$$f_{ee} = \frac{1}{(2\pi^2)^2} \left[\frac{1}{|\mathbf{p}_0 - \mathbf{p}_f|^4} - \frac{1}{|\mathbf{p}_0 - \mathbf{p}_a|^2 |\mathbf{p}_0 - \mathbf{p}_f|^2} + \frac{1}{|\mathbf{p}_0 - \mathbf{p}_s|^4} \right] . \quad (5)$$

Under these conditions, the Mott cross section does not depend on the "nature" of the electron's initial state, whether an s, p, d, or f orbital, localized or delocalized over two or more atoms of a molecule or solid. In other words the $(e,2e)$ cross section depends only on the factor $|\phi_a(\mathbf{q})|^2$, which characterizes the electron momentum density of the target, and on a factor that depends only on experimental conditions. This contrasts sharply with the measurements of photoemission by dipole transitions, whose cross sections depend in a more complicated way on momentum (see, for example, Scofield, 1976), and in which electron densities, either in coordinate or momentum space, are inaccessible to direct measurements. That all electrons contribute to $(e,2e)$ experiments greatly simplifies quantitative measurements of momentum densities. On the other hand, the matrix-element dependence of a photoemission experiment proves advantageous by allowing experimenters to "tune in" to certain electron states, by selecting the photon energy.

In the (theoretically) simplest case of the hydrogen atom ground state, the momentum density known precisely from theory has been measured accurately by Lohmann and Weigold (1981), whose results, shown in Fig. 1, demonstrate a perfect agreement between experiment and theory. The experiment was repeated for different energies of the incoming electron, as indicated in the figure, with results coinciding for all energies. This provides an experimental confirmation of the soundness of the $(e,2e)$ technique for the measurement of momentum profiles, since the observed momentum densities are independent of experimental conditions. Experiments on more complicated atoms and molecules corroborate this picture, yielding good agreement between experiment and theory if the theoretical approximations are made correctly, as reviewed by McCarthy and Weigold (1991).

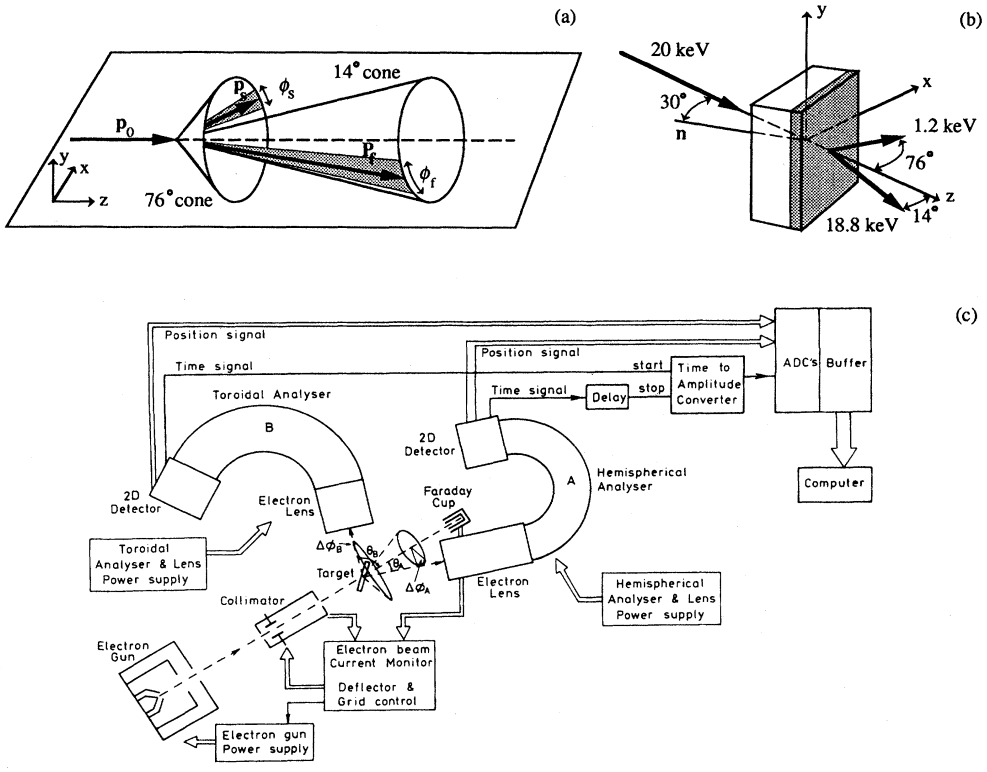

FIG. 2. The experimental configuration of a solid $(e,2e)$ spectrometer: (a) The kinematics of the experiment. The incoming beam $\mathbf{p}_0$ scatters, and the slow and fast electrons with momentums $\mathbf{p}_s$ and $\mathbf{p}_f$, respectively, are detected over a range of angles ϕ_s and ϕ_f. (b) The trajectories of the electron involved relative to the actual target. Because of the low mean free path associated with the slow (1.2 keV) electron, information obtained is almost exclusively restricted to $(e,2e)$ events occurring in the outermost (shaded) layer. (c) The analyzer setup.

III. EXPERIMENTAL APPARATUS

A major experimental difficulty arises in $(e,2e)$ experiments on solids. Measuring the complete momentum density $|\phi(\varepsilon,\mathbf{q})|^2$ (down to $\mathbf{q}=0$), utilizing momentum conservation, requires experimenting in transmission rather than reflection from the target. The target should thus be an extremely thin ($\simeq 100$ Å) foil, implying a significant probability that incident high-energy electrons will experience *single* interaction with the target. However, high energy (20 keV in our case) implies low values of the Mott cross section [Eq. (5)] and hence of the $(e,2e)$ count rate. For this reason, $(e,2e)$ spectroscopy on solids has been relatively unsuccessful compared to gas-phase experiments on atoms and molecules. Recent advances in detector technology have made $(e,2e)$ on solids a practical research tool, as described in detail by Storer *et al.* (1994) and depicted in Fig. 2. In the back focal plane of each analyzer lie two microchannel plates and a two-dimensional position-sensitive detector. One dimension of this detector corresponds to different azimuthal angles of the emerging electrons, the other to different energies. Electrons emerging from the target are thus detected over a range of angles and energies, greatly increasing the data collection rate. An $(e,2e)$ experiment can now be completed in a few days, rather than months. This effect is further enhanced by choosing an asymmetric geometry (detectors at 14° and 76°, rather than both at 45°) for which momentum transfer is smaller, and hence the cross section [Eq. (5)] is larger. As a further consequence of this configuration, the ejected electrons have a low energy (and hence a small mean free path), which makes this setup especially sensitive to the properties of the surface facing the slow-electron analyzer.

IV. FROM ATOMS TO SOLIDS

In order to make the connection between the well-tested theory of $(e,2e)$ spectroscopy of molecules and the expected $(e,2e)$ results for solids, we performed model calculations on hypothetical linear chains of hydrogen atoms of different length. The fact that these molecules are not stable in nature does not make the calculation of their properties any more difficult, and therefore we expect the calculated $(e,2e)$ spectra to resemble those one would measure if these molecules existed.

The calculations were done using the GAMESS program as described by Schmidt *et al.* (1990). In this program a Hartree-Fock-type calculation is performed, with the atomic hydrogen wave function expressed as a sum of five Gaussian-type basis functions. From the eigenvectors of the molecular orbitals we calculate the momentum-space wave function $\phi_a(\mathbf{q})$ for each orbital a. The program takes into account the electron spin, assigning two electrons to each occupied orbital (for molecules with an even number of electrons). The nearest-neighbor internuclear distance equals that of molecular hydrogen (1.4 a.u.).

Molecules of increasing length are expected to behave more and more like one-dimensional solids. Let us first establish how long a chain should be before the experimental results would become indistinguishable from those of an infinitely long chain. Figure 3 achieves this goal by plotting the normalized momentum density $|\phi_a(q_z)|^2$ with q_z directed along the axis of the molecules for the different orbitals of our "molecules." Only half of each plot is shown, as $|\phi_a(q_z)|^2$ is an even function of q_z. Thus the H_2 orbital is the same as one could measure for molecular hydrogen, provided all the molecules were aligned along the same axis. In practice, Weigold *et al.* (1977) found that random orientation of hydrogen molecules yields a measured momentum profile well described by the spherical average of the calculated momentum density.

For H_4 with two occupied orbitals, the one with the higher binding energy has a momentum wave function peaked at 0 a.u., and that with lower binding energy has a momentum wave function peaked at larger momentum values. For the lowest-energy orbital, the contributions of each atomic orbital add up in phase with each other, causing a rather flat wave function in coordinate space whereby the wave function peaks for small momentum values (as the momentum-space wave function relates to the derivative of the coordinate-space wave function).

Adding more and more atoms to the chain causes the momentum distribution of each orbital to become increasingly peaked. Again the less-bound orbitals have maximum amplitude of the wave function at larger momenta. The orbital would resemble in shape a delta function for an infinitely long chain.

The orbitals also become more and more closely spaced in energy with peaks of $|\phi_a(q_z)|^2$ roughly centered at q_z values of $\sqrt{2m^*(\varepsilon_a-\varepsilon_0)}$, where ε_0 represents the energy of the most tightly bound orbital and where m^* is the effective mass of the electron, not necessarily equal to the mass of the free electron because of the influence of the lattice. From a spectroscopic point of view, these chains would be infinitely long if the peak's width in momentum drops below the experimental momentum resolution *and* the orbitals' energy separation below the energy resolution. One would then observe experimentally a continuous distribution ("band") resembling a parabola. For our present spectrometer (momentum resolution $\simeq 0.15$ a.u., energy resolution $\simeq 2$ eV), this result would be attained at H_{32}.

For large N, the sum over all orbitals a with energy ε_a between E and $E+\Delta E$,

$$\sum_{E<\varepsilon_a<E+\Delta E} \frac{|\phi_a(\mathbf{q})|^2}{N\Delta E}, \tag{6}$$

becomes independent of N. This quantity, the spectral momentum density $|\phi(\varepsilon,\mathbf{q})|^2$, is to be calculated for solids and compared to the experimental results.

Figure 4 shows the momentum density for H_{32} summed over all occupied orbitals. Again $\mathbf{q}$ is directed

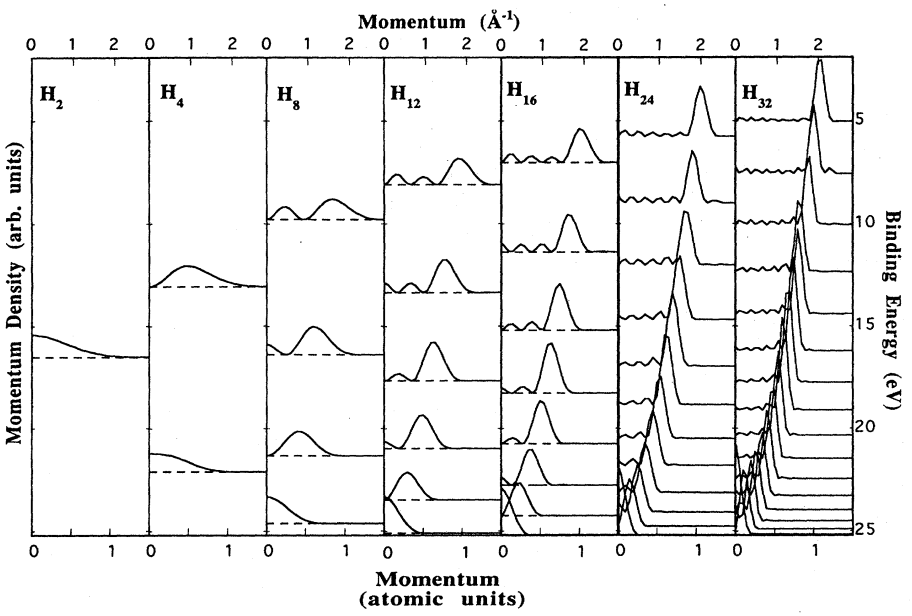

FIG. 3. Shape of the momentum density of the different molecular orbitals for hydrogen chains of different lengths, as calculated by the GAMESS program. The momentum distributions are offset by an amount proportional to the binding energy of the orbitals, as indicated on the right vertical axis. Note that the momentum distributions become more and more peaked with increasing length of the chain. Also the peak positions shift slowly to higher momentum values with increasing binding energy.

along the molecular axis. The shape of this plot differs completely from that determined for atomic H, shown here as well as in Fig. 1 and normalized to equal area. The H_{32} plot remains fairly constant for small momenta, exhibits a maximum near 0.7 a.u., and drops off sharply near 1.12 a.u. A free-electron gas would yield a constant density up to a value $\mathbf{k}_f$ and zero density beyond this value. Thus, except for the maximum near 0.7 a.u. (possibly related to the finite size of the H_{32} molecule), the summed momentum density resembles that of a free-electron gas rather than that of a hydrogen atom.

A simple interpretation of the wave functions $\phi_a(q_z)$ of

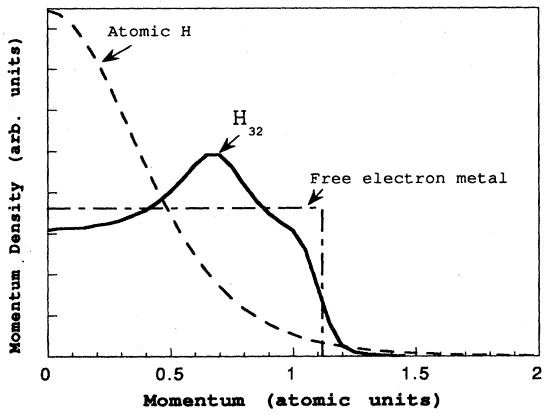

FIG. 4. Momentum density of the H_{32} molecule as obtained by summing over all occupied orbitals of this molecule as shown in Fig. 3. Also shown are the theoretical density for a free-electron metal with $\mathbf{k}_f$ chosen to be 1.12 a.u. and the one for atomic hydrogen. All curves are normalized to equal area. The momentum density of the chain resembles more the free-electron case than that of atomic hydrogen.

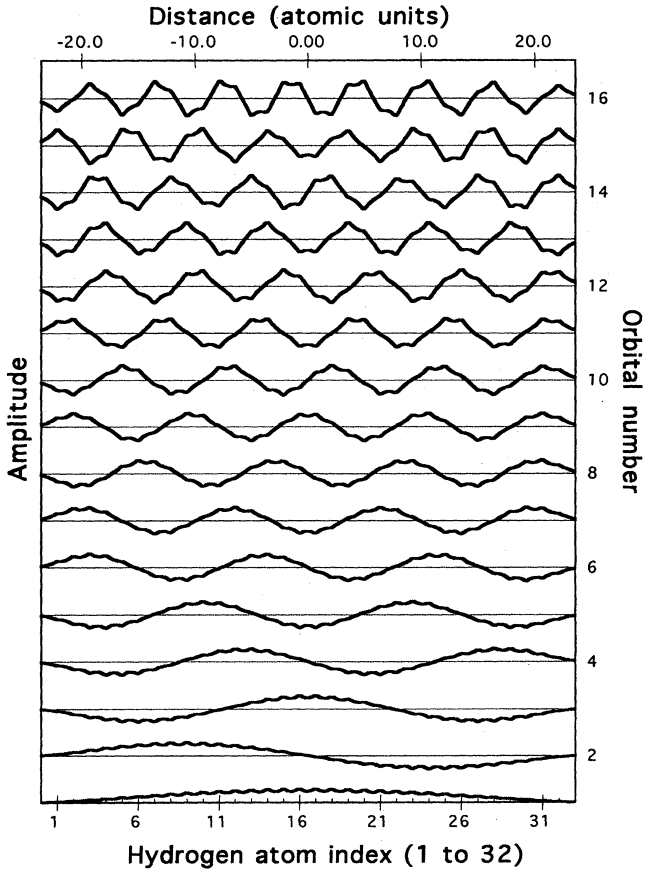

FIG. 5. Coordinate-space wave functions for H_{32}, with orbitals numbered from 1 to 16 with decreasing binding energy. Note the resemblance of the functions for H_{32} with those of the "particle in the box" problem.

different H_{32} orbitals emerges when we transform $\phi_a(q_z)$ into $\psi(z)$ in coordinate space as shown in Fig. 5. The wave functions resemble solutions of the "particle in a box" problem, with the electrons behaving like free electrons in a one-dimensional box with the chain's length. The relation between momentum and energy is thus found to be $\varepsilon=\varepsilon_0|\mathbf{q}|^2/2m^*$. Close inspection of the wave function shows some modulation with the periodicity of the hydrogen lattice, indicating that the potential is modulated at the bottom of the box by the nuclei at the lattice sites. To summarize, one would describe an infinitely long one-dimensional H chain in solid-state language as a nearly-free-electron metal with a single band. Taking into account the electron spin leaves this band half-filled (0.5 orbitals per unit cell).

V. COMPARING THE MODEL DENSITIES WITH MEASUREMENTS ON ACTUAL METALS

It is interesting to compare the results for the hydrogen chain with the densities as measured for the nearly-free-electron metal aluminum. A thin film ($\simeq$40 Å) of Al was evaporated on a 50-Å amorphous carbon film (Canney *et al.*, 1995). The small mean free path of the slow electron suppressed the signal of the amorphous carbon backing, to the extent of burying it in the noise. The aluminum signal stood out clearly. Whereas Fig. 3 showed only the positive momenta q, because the momentum density is symmetric with respect to the origin, the experimental data shown in Fig. 6 include the momentum density along both the positive and the negative axis. Zero value of the binding energy corresponds to the vacuum level. The Fermi level lies near 5 eV binding energy (indeed, the measured coincidence rate drops quickly to zero for smaller binding energies). The two peaks at each energy approach each other with increasing binding energies, merging around 16 eV. Residual intensity at larger binding energy is due to events that have experienced additional energy-loss processes (e.g., plasmon excitations). The qualitative resemblance of the Al data and the H_{32} calculations is striking. This figure

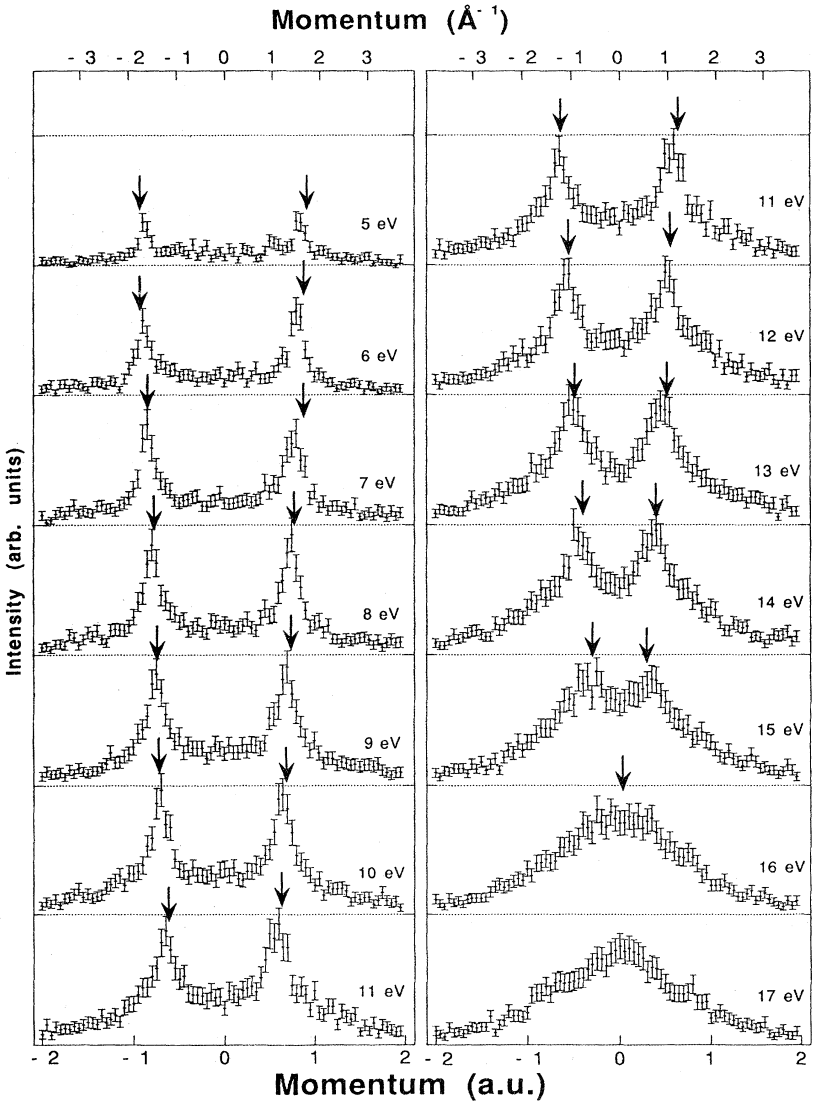

FIG. 6. The momentum density of electrons of an aluminum film at different values of ε. Binding energies are referred to the vacuum level. The Fermi level lies at $\simeq$4.5 eV. Arrows indicate the expected momentum peak positions for a free-electron gas at each energy.

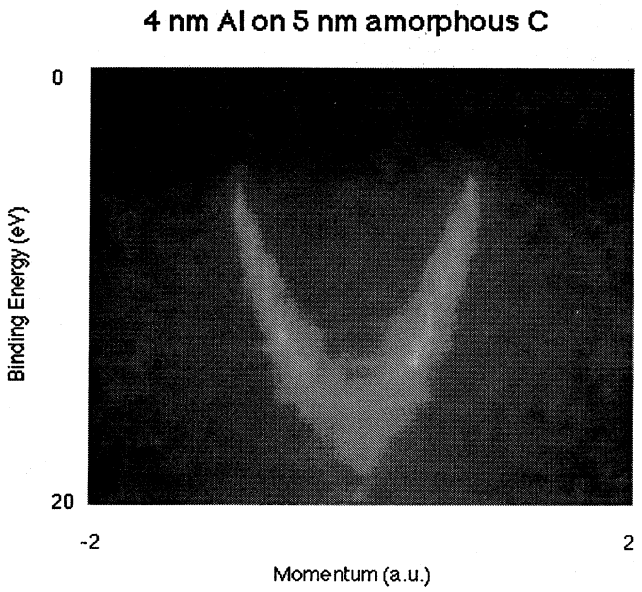

FIG. 7. The spectral momentum density of aluminum shown as a grey-scale plot. The lighter the shading, the greater the intensity. Inelastic energy-loss effects have been deconvoluted. Note the parabolic shape of the band.

also indicates the expected peak position for a free-electron solid (effective mass equals the free-electron mass, at an inner potential of 16 eV below the vacuum level). Figure 7 presents the same data as a grey-scale plot with the data corrected approximately by a deconvolution procedure for inelastic energy losses. The lower the shading, the higher the intensity. Again a free-electron parabola is clearly visible, with a fairly constant intensity over the parabola, as expected for a free-electron metal.

VI. THE EFFECTS OF UNIT CELL SIZE ON THE MOMENTUM DENSITIES

Let us now consider again the chain of thirty-two hydrogen atoms. If we make the unit cell twice as big by alternating shorter and longer distances between hydrogen atoms, we have sixteen unit cells. Now the wavelength of the sixteenth orbital, which is the least-bound occupied orbital $\psi_{16}(z)$ in Fig. 5, would correspond to twice the unit cell length. The charge density $|\psi_a(z)|^2$ would oscillate with half this wavelength. In an infinitely long chain, orbitals at this wavelength could have either maximum density $|\psi_a(z)|^2$ near the center of gravity of the positive charge of the unit cell, or, by changing the phase by 90°, minimum charge density at this position. These two orbitals have clearly quite different energies. Thus there is a sudden jump in energy as a function of $\mathbf{q}$ for momentum values of $0.5\mathbf{G}$. This jump is referred to as the band gap, and in this case of a modulated H chain it lies right at the Fermi level. Such a crystal is a semiconductor. Figure 8 shows results of calculations of this gap for modulations of different strengths. (Interatomic distances of 1.6 and 1.2 a.u. for weak modulations and 1.8 and 1.0 a.u. for strong modulations, leaving the overall length of the chain approximately constant). Indeed, these calculations show that the topmost orbitals of H_{32} are lowered in energy, with a gap opening up at the Fermi level, the effect being strongest for the largest modulation. From band theory we know that band gaps open up as the band crosses the Brillouin-zone boundary. The first Brillouin-zone boundary is at half a reciprocal-lattice vector $\mathbf{G}$ and is shown by a vertical dashed line in the plot (unit cell length $1.6+1.2=2.8$ a.u., $0.5\times\mathbf{G}=0.5\times 2\pi/2.8\simeq 1.1$ a.u.)

The solid line in this figure connects the energies with maximum intensity of $|\phi_a(\mathbf{q})|^2$. This line would correspond to the dispersion curve of the band in the first Brillouin zone. If we drew the band structure in the extended zone scheme, we would have to add a branch of the band in the negative half of the first Brillouin zone (not shown in the drawing), shifted by one reciprocal-lattice vector $\mathbf{G}$. This is shown as a dotted line. Note that this line connects a series of secondary maxima in $|\phi_a(\mathbf{q})|^2$ which are most pronounced near the Brillouin-zone boundary.

Let us now stress a major difference between a chain of finite length and an infinitely large crystal. In a chain of finite length the traveling waves will reverse at the boundaries and standing waves form with both momenta $\mathbf{q}$ and $-\mathbf{q}$. In an infinite crystal there are no boundaries, and the wave function is described either by $\mathbf{q}$ or $-\mathbf{q}$. Thus the secondary maxima in Fig. 8 can be interpreted as the main $-\mathbf{q}$ component shifted by a reciprocal-lattice vector $\mathbf{G}$ due to interaction with the lattice. For an infinite crystal it would only be part of the wave function with its main component at $-\mathbf{q}$. Note that the secondary maxima are larger for the strongly modulated case, as expected because the lowest Fourier component will be stronger here.

Generalizing this picture for a crystal leads to the following important conclusion. When the eigenfunctions are described as Bloch functions [Eq. (1)], $(e,2e)$ data should determine the magnitude of the coefficients $c_{\mathbf{G}}$. Clearly this cannot be done with a spectroscopy that relies on the reduced zone scheme, as all vectors $\mathbf{q}+\mathbf{G}$ are equivalent here.

Let us compare the results of our "semiconductor hydrogen chain" with the measured $(e,2e)$ spectra of a real-life semiconductor, Si. Figure 9(a) shows the measured spectral momentum density of silicon in a grey-scale plot. The lighter shading corresponds to momentum-energy combinations of high intensities. Indeed, the plot resembles that of the H chain with two atoms per unit cell. Next to the experimental density we have plotted, in a similar way, the theoretical spectral

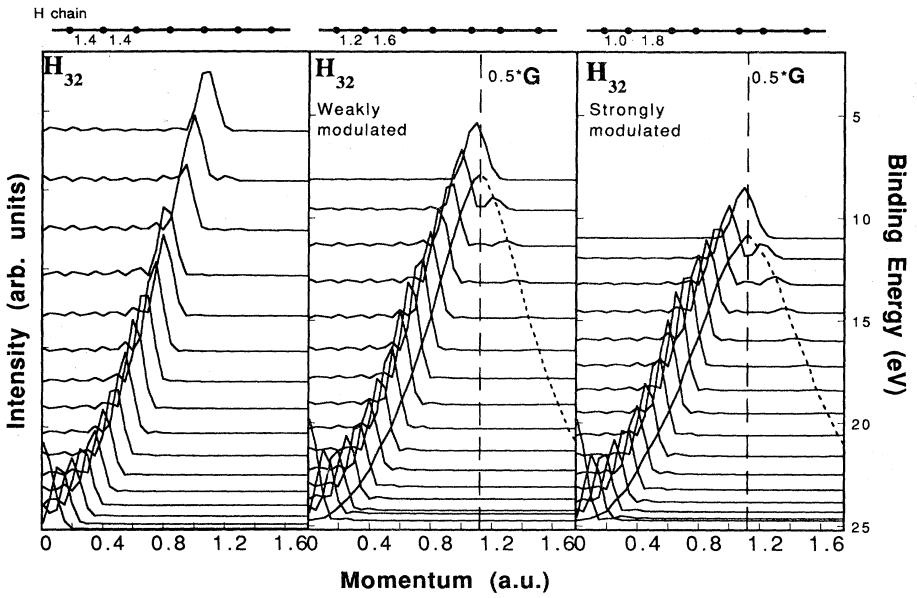

FIG. 8. The momentum density for H_{32} (identical to Fig. 3) and for the same molecule with modulation of the internuclear spacing as described in the text. Also shown is the momentum value corresponding to half a reciprocal-lattice vector (vertical line). The thick solid line represents the band shape as inferred from the peak positions of the orbitals. The thick dotted line indicates the band plotted in the "repeated zone" scheme.

momentum density. These calculations were done using the linear-muffin-tin-orbital approach as described by Skriver (1984). Note that the measured and calculated dispersions are almost identical; in both cases the dispersion curve flattens out at 1.0 a.u. For details, see Vos, Storer, *et al.* (1995a).

We now enlarge our unit cell by another atom. The interatomic distances were set in a pattern *a-a-b-a-a-b-a* etc., with $a = 1.6$ a.u. and $b = 1.0$ a.u., for H_{36}, i.e., with 12 unit cells. Thus there are now three electrons per unit cell, filling the first band completely (two electrons) and half of the second band (one electron). These results are

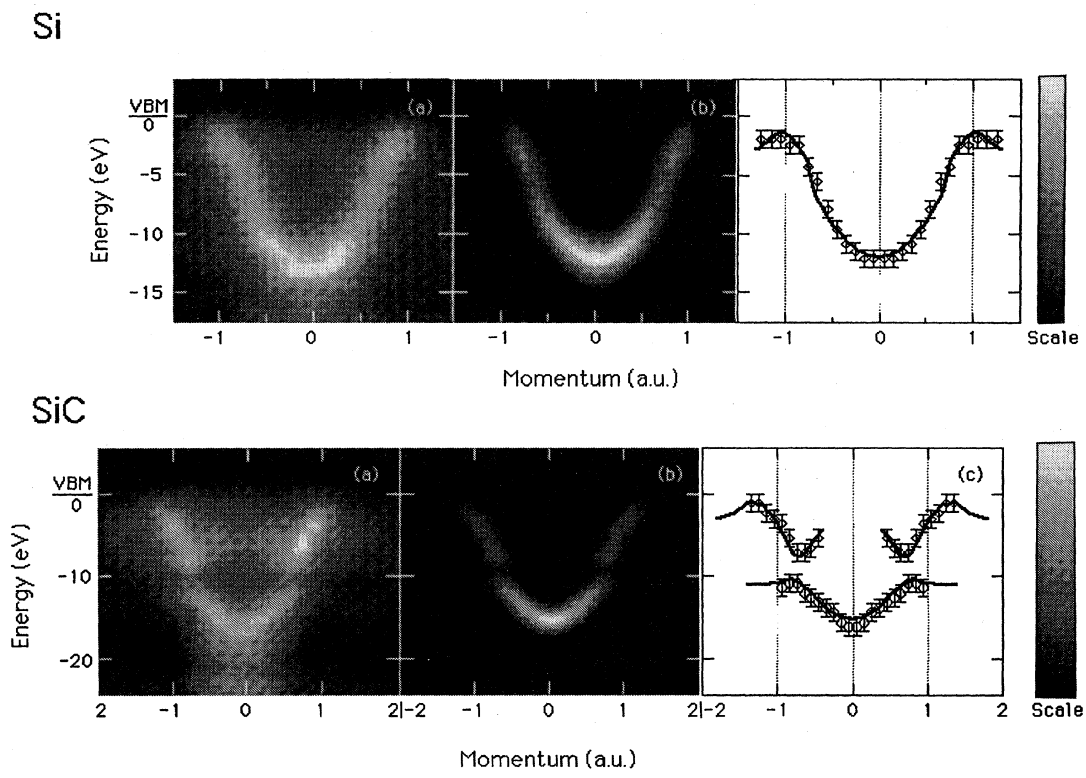

FIG. 9. A comparison of the experimental spectral momentum densities with theory for Si and SiC: (a) A grey-scale plot of the measured spectral momentum density of amorphous silicon. The lighter the shading, the larger the intensity. (b) The calculated spectral momentum density of polycrystalline silicon. (c) Comparison of experimental and theoretical dispersion relations, from Vos, Storer, *et al.* (1995a). The data for SiC are presented in the lower panel in a similar way. In this case there is a band gap around 10 eV binding energy (from Cai *et al.*, 1995b).

shown in Fig. 10(a). The main trend is as expected: an inner band disperses towards the first Brillouin-zone boundary, with smaller peaks on the right side of the Brillouin-zone boundary. The second band starts in the second Brillouin zone at energies separated from the first band by a clear gap.

However, one notices that the lower band has only 11 orbitals, whereas it is expected for a completely filled band that this number will equal the number of unit cells. The second band seems to start unexpectedly with two orbitals with almost the same energy, and these two orbitals have significant momentum tails extending to zero momentum. The nature of these deviating orbitals becomes obvious as we plot the wave function in coordinate space [Fig. 10(b)]. Orbitals 12 and 13 are the ones with almost equal energy. The electrons associated with these orbitals are located mainly near the end of the chain, i.e., we have created a one-dimensional equivalent of a surface state with an energy in the band gap. This is a well-known phenomenon in semiconductor physics. Thus in this model with 18 orbitals, 11 are part of the inner band, 5 are part of the second band, and 2 are associated with a localized electron at the end of each chain.

Note again that $(e,2e)$ spectroscopy should determine the electron distribution among the Brillouin zones, i.e., our measurement is not in the reduced zone scheme, but rather in the extended zone scheme.

Figure 9(b) shows results for SiC obtained by Cai *et al.* (1995b) as an example of a solid displaying two separate filled bands separated by a clear gap. This gap is absent for silicon, for symmetry reasons peculiar to solids in three dimensions (see Heine, 1960, for a detailed explanation). Indeed, a gap appears in the spectral momentum density of SiC, as it does for three hydrogens per unit cell. Note also traces of the secondary maxima. This is a clear demonstration that $(e,2e)$ indeed measures in the

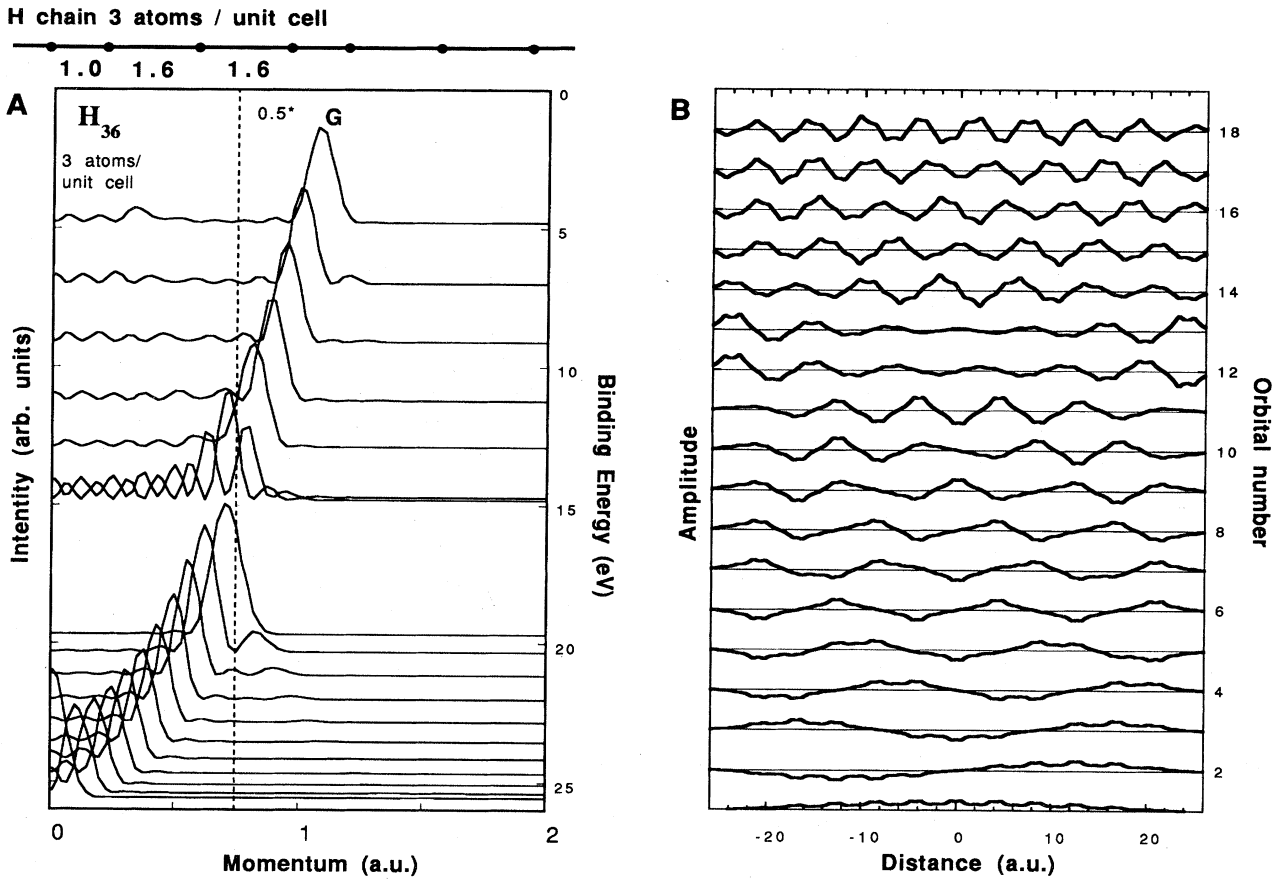

FIG. 10. The electronic structure of a hydrogen chain with three atoms per unit cell: (a) Momentum densities of different orbitals, plotted in a fashion similar to that of Fig. 3 for a chain of 36 hydrogen atoms with three atoms per unit cell. Note the band gap at the crossing between the momentum corresponding to maximum intensity of the orbitals and the Brillouin-zone boundary (dotted vertical line). Note also the two orbitals with almost identical binding energy (15 eV), with large momentum tails extending to zero momentum. (b) The wave functions in coordinate space. The two peculiar orbitals (Nos. 12 and 13) lie at the end of the chain and correspond to the one-dimensional equivalent of surface gap states.

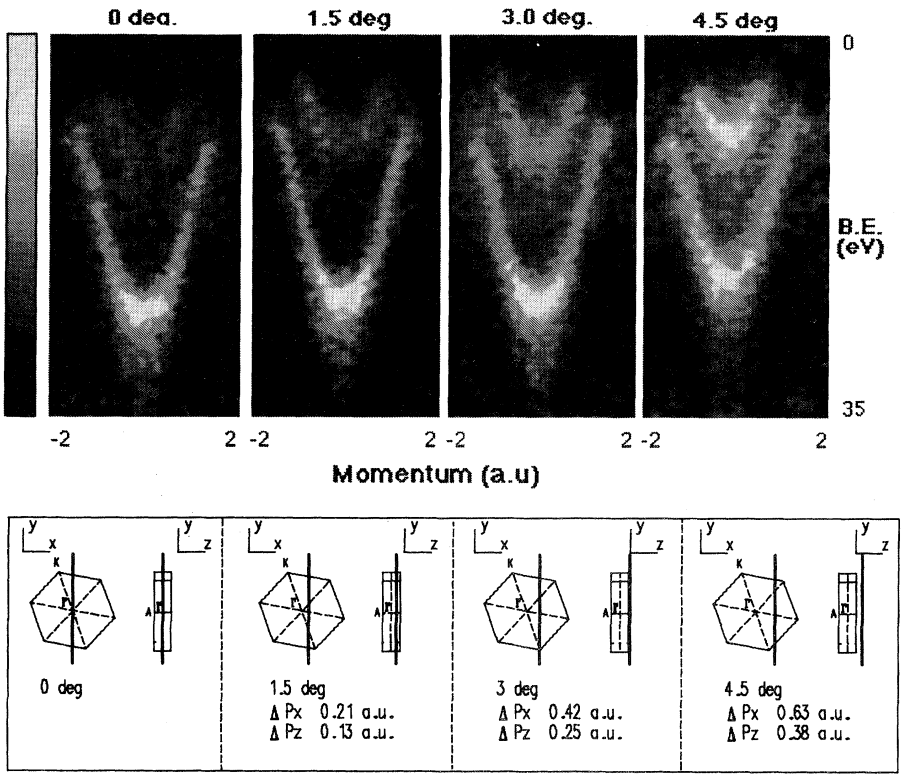

FIG. 11. The measured spectral momentum density for graphite. In the experiment one detector was rotated by the indicated amount. This caused a shift of the line along which the spectral momentum density was determined in the Brillouin zone, away from Γ as indicated in the lower half. The intensity of the upper (π) band increases as one moves out of the $\Gamma-K$ plane.

extended zone scheme.

The samples of Si and SiC discussed here were not single crystals. The Si sample was made by evaporation, yielding amorphous Si, the SiC sample by annealing a Si layer on top of a carbon film. The latter seems to consist of small crystallites, with an additional complication due to the possible presence of different phases (allotropes). Nevertheless, $(e,2e)$ shows a nice dispersion relation. This is expected for polycrystalline solids, in which the effective mass of the electron is isotropic (i.e., the effective mass tensor averages to a scalar) and for amorphous solids with a fair amount of short-range order.

VII. $(e,2e)$ MEASUREMENT OF AN ANISOTROPIC SOLID

Graphite is the only true single crystal studied thus far by $(e,2e)$ spectroscopy. The first experiment by Gao *et al.* in 1988 showed dispersion, with quantitative comparison hampered by poor statistics, but a more detailed comparison was afforded by improved statistics and resolution in the second experiment by Vos *et al.* (1995a). At the energies used in these $(e,2e)$ experiments, the refraction effects at the surface of the crystal were small and we were not restricted to measuring the electronic structure in the plane parallel to the surface. This is especially interesting for the case of graphite, a layered material with completely different electronic bonding within a plane (strong, covalent) and between planes (weak, mainly van der Waals type bonding). This is reflected in the two bands present, referred to as σ and π bands. In Fig. 11 we show the spectral momentum density for measurements along different lines in the Brillouin zone, as indicated schematically. Measurements along the different lines were achieved experimentally by rotating one of the detectors. For spectra with no momentum component perpendicular to the basal plane, the π band should have zero intensity and only the σ band should be visible. In practice, there is still a trace of the π band left (due probably to finite momentum resolution), but it becomes more and more intense if we measure in configurations that correspond to higher and higher momentum components perpendicular to the basal plane.

VIII. SUMMARY AND OUTLOOK

We have described how the $(e,2e)$ spectrum of a molecule, indicating the momentum distribution of discrete orbitals, evolves into the $(e,2e)$ spectrum of a solid whose momentum distributions extend over a continuous band of energies. The relation between the measured quantities in an $(e,2e)$ spectrum and those used in the description of crystals in terms of band structures has been outlined. In particular, we have discussed the consequences of measuring real momentum rather than crystal momen-

tum. Finally, we have shown some experimental results.

In the future we hope to be able to enhance the energy resolution of this technique to 0.5 eV. Advances in target preparation techniques should allow us to measure a larger range of targets. The fact that $(e,2e)$ can measure dispersion relations and the corresponding electron momentum densities in solids is clear. We mentioned briefly the application of $(e,2e)$ to amorphous solids, where experimental tests of the electronic structure seem feasible, especially with enhanced resolution, and when thin crystalline targets become available for comparison. Finally we have not even begun to explore the field of electron-electron correlation in solids, an area where $(e,2e)$ spectroscopy has contributed significantly to the study of atoms and molecules.

ACKNOWLEDGMENTS

The authors want to thank the technical staff of the Electronic Structure of Materials Centre for their indispensable contributions to the construction of the $(e,2e)$ spectrometer. We are grateful to Y. Q. Cai, S. Canney, A. S. Kheifets, P. Storer, S. Utteridge, and E. Weigold for many stimulating discussions and critical reading of the manuscript. The Electronic Structure of Materials Centre is supported by a grant of the Australian Research Council.

REFERENCES

Amaldi, U., Jr., A. Egidi, R. Marconero, and G. Pizzella, 1969, Rev. Sci. Instrum. **40**, 1001.

Cai, Y. Q., M. Vos, P. Storer, A. S. Kheifets, I. E. McCarthy, and E. Weigold, 1995a, Solid State Commun. **95**, 25.

Cai, Y. Q., M. Vos, P. Storer, A. S. Kheifets, I. E. McCarthy, and E. Weigold, 1995b, Phys. Rev. B **51**, 3449.

Camilloni, R., A. Guardini-Guidoni, R. Tiribelli, and G. Stefani, 1972, Phys. Rev. Lett. **29**, 618.

Canney, S. A., M. Vos, P. Storer, A. S. Kheifets, I. E. McCarthy, and E. Weigold, 1995, unpublished.

Caprari, R. S., S. A. C. Clark, I. E. McCarthy, P. Storer, M. Vos, and E. Weigold, 1994, Phys. Rev. B **50**, 12078.

Coplan, M. A., J. H. Moore, and J. P. Doering, 1994, Rev. Mod. Phys. **66**, 985.

Egerton, R. F., 1986, *Electron Energy Loss Spectroscopy in the Electron Microscope* (Plenum, New York).

Gao, C., A. L. Ritter, J. R. Dennison, and N. A. W. Holzwarth, 1988, Phys. Rev. B **37**, 3914.

Hayes, P., J. F. Williams, and J. Flexman, 1991, Phys. Rev. B **43**, 1928.

Heine, V., 1960, *Group Theory in Quantum Mechanics* (Pergamon, Oxford), Chap. 6.

Levin, V. G., V. G. Neudachin, and Yu. F. Smirnov, 1972, Phys. Status Solidi **49**, 489.

Lohmann, B., and E. Weigold, 1981, Phys. Lett. A **86**, 139.

McCarthy, J. E., and E. Weigold, 1991, Rep. Prog. Phys. **54**, 789.

Neudachin, V. G., G. A. Novoskoltseva, and Yu. F. Smirnov, 1968, Zh. Eksp. Teor. Fiz. **55**, 1039 [Sov. Phys. JETP **28**, 540 (1969)].

Persiantseva, N. M., N. A. Krasil'nikova, and V. G. Neudachin, 1979, Sov. Phys. JETP **49**, 530.

Ritter, A. L., J. R. Dennison, and R. Jones, 1984, Phys. Rev. Lett. **53**, 2054.

Schmidt, M. W., K. K. Baldridge, J. A. Boatz, J. H. Jensen, S. Koseki, M. S. Gordon, K. A. Nguyen, T. L. Windus, and S. T. Elbert, 1990, Quantum Chem. Program Exchange Bull. **10**, 52.

Scofield, J. H., 1976, J. Electron. Spectrosc. **8**, 129.

Skriver, H. L., 1984, *The LMTO Method* (Springer, New York).

Storer, P., S. A. C. Clark, R.C. Caprari, M. Vos, and E. Weigold, 1994, Rev. Sci. Instrum. **65**, 2214.

Vos, M., S. A. Canney, A. S. Kheifets, I. E. McCarthy, and E. Weigold, 1995a, unpublished.

Vos, M., S. A. Canney, P. J. Storer, I. E. McCarthy, and E. Weigold, 1995b, Surf. Sci. **327**, 3007.

Vos, M., P. Storer, Y. Q. Cai, A. S. Kheifets, I. E. McCarthy, and E. Weigold, 1995a, J. Phys. Condens. Matter **7**, 279.

Vos, M., P. J. Storer, Y. Q. Cai, I. E. McCarthy, and E. Weigold, 1995b, Phys. Rev. B **51**, 1866.

Vos, M., P. Storer, S. A. Canney, A. S. Kheifets, I. E. McCarthy, and E. Weigold, 1994, Phys. Rev. B **50**, 5635.

Weigold, E., I. E. McCarthy, A. J. Dixon, and S. Dey, 1977, Chem. Phys. Lett. **47**, 209.

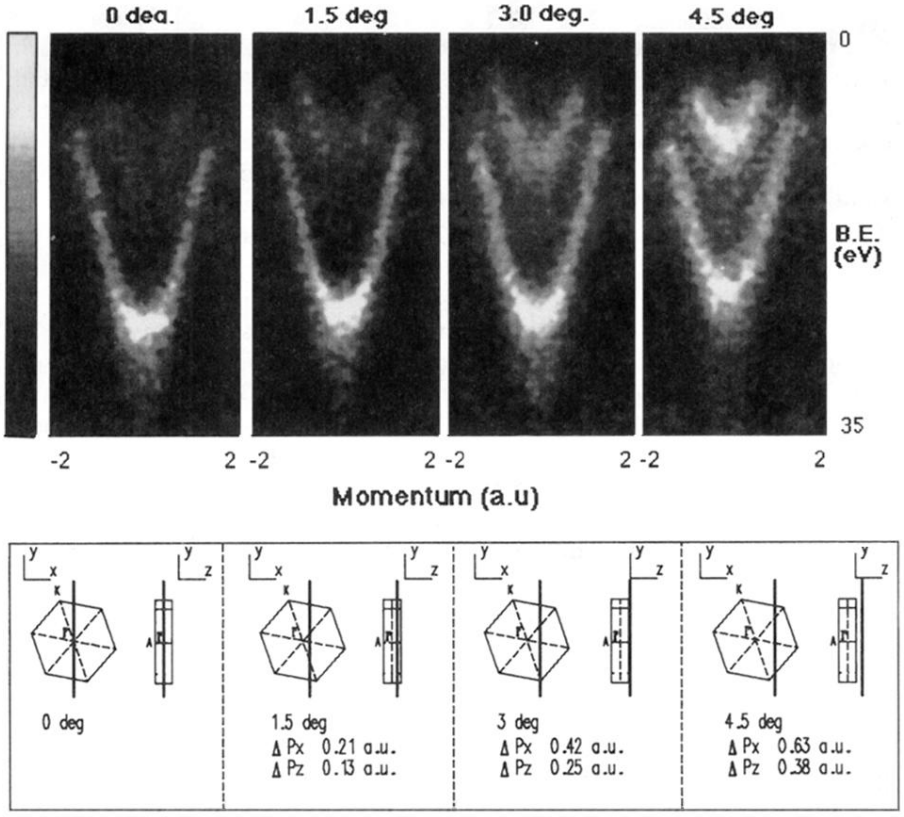

FIG. 11. The measured spectral momentum density for graphite. In the experiment one detector was rotated by the indicated amount. This caused a shift of the line along which the spectral momentum density was determined in the Brillouin zone, away from Γ as indicated in the lower half. The intensity of the upper (π) band increases as one moves out of the $\Gamma - K$ plane.

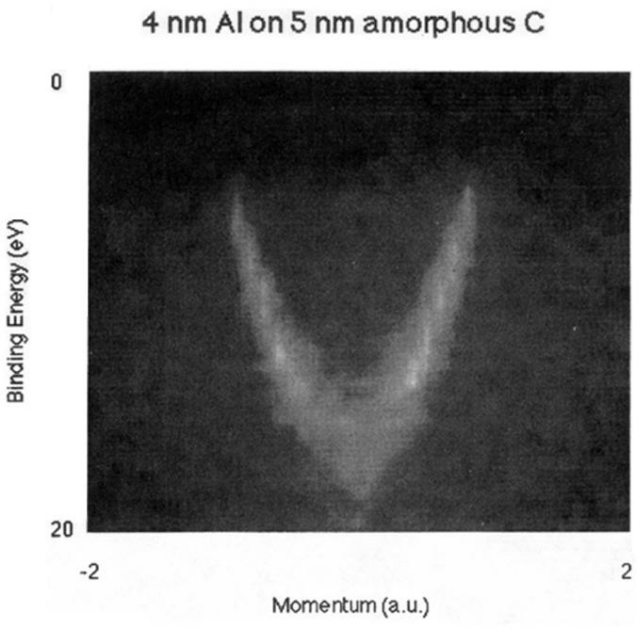

FIG. 7. The spectral momentum density of aluminum shown as a grey-scale plot. The lighter the shading, the greater the intensity. Inelastic energy-loss effects have been deconvoluted. Note the parabolic shape of the band.

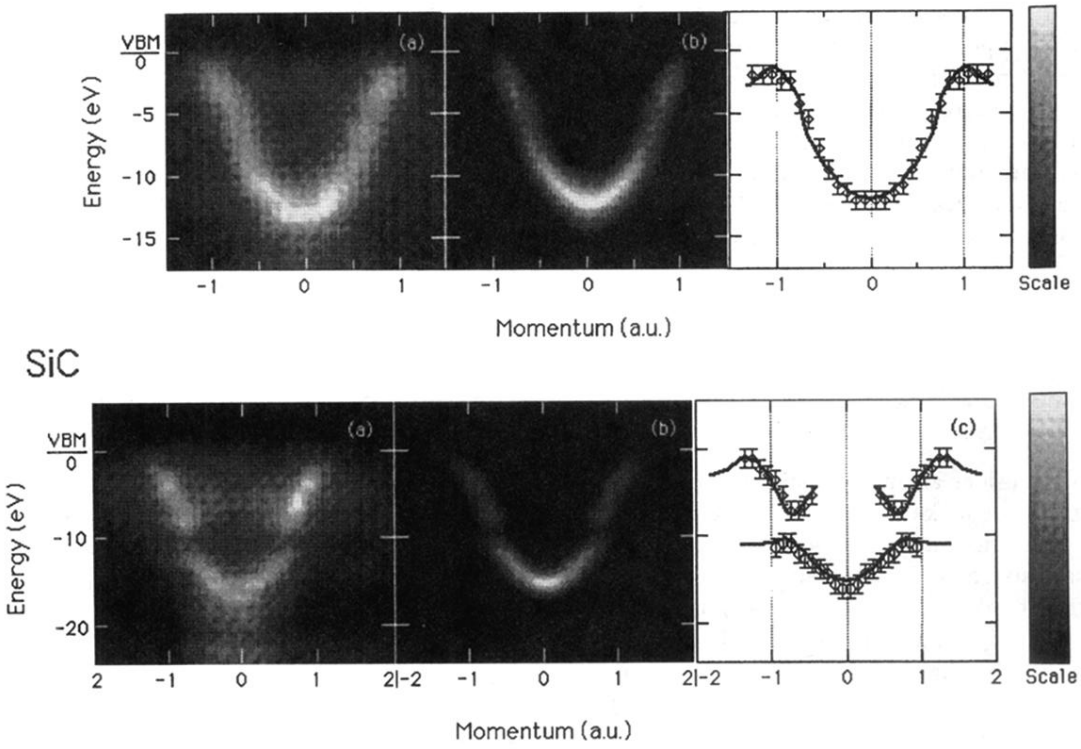

FIG. 9. A comparison of the experimental spectral momentum densities with theory for Si and SiC: (a) A grey-scale plot of the measured spectral momentum density of amorphous silicon. The lighter the shading, the larger the intensity. (b) The calculated spectral momentum density of polycrystalline silicon. (c) Comparison of experimental and theoretical dispersion relations, from Vos, Storer, *et al.* (1995a). The data for SiC are presented in the lower panel in a similar way. In this case there is a band gap around 10 eV binding energy (from Cai *et al.*, 1995b).